A practical workflow for road slopes monitoring using handled mobile mapping systems

José Miguel Gómez-López [1], José. Luis Pérez-García [1], Antonio Tomás Mozas-Calvache [1], Jorge Delgado-García[1], Diego Vico-García[1]

[1] Dept. Ing. Cartográfica, Geodésica y Fotogrametría, University of Jaén, 23071 Jaén, Spain - (jglopez, jlperez, antmozas, jdelgado, dvico)@ujaen.es

Keywords: Mobile Mapping Systems (MMS), LiDAR, point cloud, road slope deformation monitoring.

Abstract

High-resolution monitoring of road infrastructure is essential for the early detection of geomorphological instabilities such as landslides and erosion. This study evaluates the performance of handled MMS under different vehicle-mounted configurations: a 2-meter survey pole versus a suction-cup mount, and varying acquisition speeds (10 and 20 km/h). Furthermore, a GNSS-denied scenario was simulated to test the robustness of SLAM-based processing. Initial results revealed significant geometric discrepancies (double-points artifacts and drift), particularly in the SLAM-only and high-speed datasets. To address this, an automated segment-based refinement workflow was developed using a ICP algorithm. The refinement successfully reduced the standard deviation to the level of the point cloud´s mean point spacing (5 cm). Comparative multitemporal analysis against UAV-LiDAR reference data confirms that the proposed refinement renders even SLAM-processed data viable for detecting centimetric terrain displacements. The findings demonstrate that while suction-cup mounting at 10 km/h is optimal, algorithmic refinement allows for reliable road slopes monitoring and change detection across all tested configurations.

1. Introduction

Landslides and rockfalls are complex geomorphological processes triggered by the fracture and movement of rock masses, sediments, or artificial fills under the direct influence of gravity (Clague, 2013). These phenomena are globally recognized as a major hazard, driven by a combination of predisposing factors and specific triggers. Seismic activity, climatic variations—most notably intense or prolonged rainfall and freeze-thaw cycles—and anthropogenic interventions such as road excavations or improper drainage are the primary drivers of slope instability. The impact of these events extends far beyond geological interest, posing a severe threat to human life and imposing a substantial economic burden on regional and national economies. In the context of road infrastructure, the disruption of transport networks leads to direct repair costs and indirect economic losses due to traffic delays and restricted accessibility. A poignant example is found in the province of Jaén, Spain. The provincial road network, managed by the local government (Diputación de Jaén), faces recurring instability issues. It is estimated that the average annual cost for damage repair on these provincial roads alone is approximately 1.6 million euros. In years characterized by extreme weather events, this figure has surged to over 10 million euros. Such high costs underscore the fact that identifying and evaluating hazards is the first and most critical strategy for risk reduction (Clague, 2013). Knowledge-driven management enables the transition from reactive maintenance to proactive prediction and intelligent decision-making, facilitating better preparation, the implementation of Early Warning Systems (EWS), and efficient post-event recovery.

Effective slope monitoring is predicated on the ability to generate high-resolution, multi-temporal three-dimensional (3D) terrain models. Historically, obtaining such data was a resource-intensive endeavor. Classic geomatic techniques required significant deployments of specialized personnel and expensive instrumentation. Both the data capture phase and the subsequent processing were time-consuming, often creating a bottleneck in the monitoring workflow. The landscape of terrain modeling has been fundamentally altered by the integration of digital photogrammetry and Light Detection and Ranging (LiDAR) with Remotely Piloted Aircraft Systems (RPAS) (Zhang and Zhu, 2023; Kovanič et al., 2023). Before the widespread adoption of RPAS, work scales were polarized: small and medium scales were the domain of manned photogrammetric flights, while large or very large scales required terrestrial-based sensors. The emergence of RPAS-based sensors has successfully bridged this gap, allowing for high-precision studies of road slopes ranging from a few dozen to several hundred meters. This technological shift has been accompanied by what authors like Westoby et al. (2012) term the "democratization of photogrammetry." The implementation of algorithms such as Structure from Motion (SfM) (Szeliski, 2011) into user-friendly software has lowered the technical barrier to entry. Modern SfM workflows allow for the simultaneous analytical calibration of cameras during processing, enabling the use of non-metric, low-cost sensors that do not require rigorous a priori calibration. Furthermore, the shift toward cloud-based processing has enabled the handling of massive datasets remotely, expanding the possibilities for territorial monitoring to a broader range of users and agencies.

Various examples in the literature demonstrate the application of these techniques for road slope monitoring, utilizing them either individually—via photogrammetry (Türk et al., 2024) or LiDAR (Mat Zam et al., 2018)—or through integrated multi-sensor approaches (Fernández et al., 2021). Furthermore, comprehensive state-of-the-art review by Sun et al. (2024) provide a detailed overview of the current capabilities and trends within this context. Despite the versatility of RPAS and traditional LiDAR, there is an increasing demand for even more agile data acquisition. In scenarios involving active landslides or emergency response, the time required for flight planning, deployment, and post-processing can be a critical limitation. This has led to the proliferation of Mobile Mapping Systems (MMS) (Elhashash et al., 2022), where mapping sensors are integrated into mobile platforms—such as vehicles, backpacks, or handheld devices—to provide continuous geospatial data collection (Al-Bayari, 2019). Modern MMS typically combine LiDAR sensors and high-resolution cameras with a suite of positioning sensors, including Global Navigation Satellite Systems (GNSS) and Inertial Measurement Units (IMU). The core of many portable MMS solutions is Simultaneous Localization and Mapping (SLAM) technology. SLAM allows a system to build a map of an unknown environment while simultaneously keeping track of its own location within that map. While visual-IMU SLAM has been extensively documented in robotics and autonomous driving (Kazerouni et al., 2022), LiDAR-SLAM techniques have recently seen a surge in interest for geomatic applications (Huang, 2021). The current frontier in this field is the development of hybrid vision-LiDAR solutions. These systems leverage the complementary strengths of both sensors: LiDAR provides precise geometry and works in varied lighting conditions, while visual data provides rich texture and semantic information. Such hybrid approaches offer superior robustness during aggressive movements or in "feature-poor" environments where single-sensor SLAM might fail (Debeunne and Vivet, 2020).

The advantage of portable MMS lies in their extraordinary flexibility and significantly reduced cost compared to traditional surveying equipment or high-end vehicle-mounted systems (Raper, 2009). However, the scientific community faces a significant hurdle: the "black-box" nature of many commercial handheld systems and a lack of transparency regarding their error budgets.

The application of low-cost MMS is often hampered by an insufficient understanding of systematic error behavior (Kalenjuk and Lienhart, 2022). Unlike traditional surveying, where errors are relatively static and well-defined, the error budget in SLAM-based MMS is dynamic, complex, and time-dependent. When trajectories are calculated without the support of costly Ground Control Points (GCPs)—a common practice to save time and labor—the resulting point clouds can exhibit drifts in the decimetric range. These drifts can occur over very short time spans and are influenced by the quality of the internal sensors (GNSS/IMU) and the complexity of the environment. For infrastructure monitoring, this level of uncertainty is critical; it becomes difficult to distinguish between actual terrain deformation (centimetric changes) and sensor-induced drift (decimetric noise), making reliable change detection a highly complex task. Current commercial vehicle-mounted MMS remain inaccessible to many local agencies due to their high cost. Conversely, while handheld or backpack systems are more affordable, their closed processing ecosystems limit the ability of researchers to model and mitigate these inherent uncertainties.

This paper presents a preliminary study aimed at defining the operational limits and scope of Handheld Mobile Mapping Systems (HMMS) for road slope monitoring. The research focuses on a comprehensive error analysis derived from different mounting configurations and data acquisition modes, specifically simulating environments with degraded or limited GNSS coverage. Consequently, the most efficient setup is proposed, alongside a robust methodology to rectify the resulting point clouds, as required, for high-precision multi-temporal studies. Finally, a comparison between two independent surveys is performed to validate the methodology and to detect active erosion and landslide phenomena affecting the slopes of the studied road section.

1.1 Case study

The study area (Figure 1a) focuses on the JA-3270 secondary road, managed by the Provincial Council of Jaén (Diputación Provincial de Jaén). Specifically, the research covers a 1.3 km section that underwent extensive remodeling in 2023 (Figure 1b). The typical cross-section of this segment comprises the road surface, embankments, and slopes of varying compositions. These include natural terrain, areas reinforced with metallic mesh, stone block riprap, and sections stabilized with shotcrete. This diverse morphological environment provides an ideal setting to test the performance of mapping technologies across different surface textures and stabilization methods.

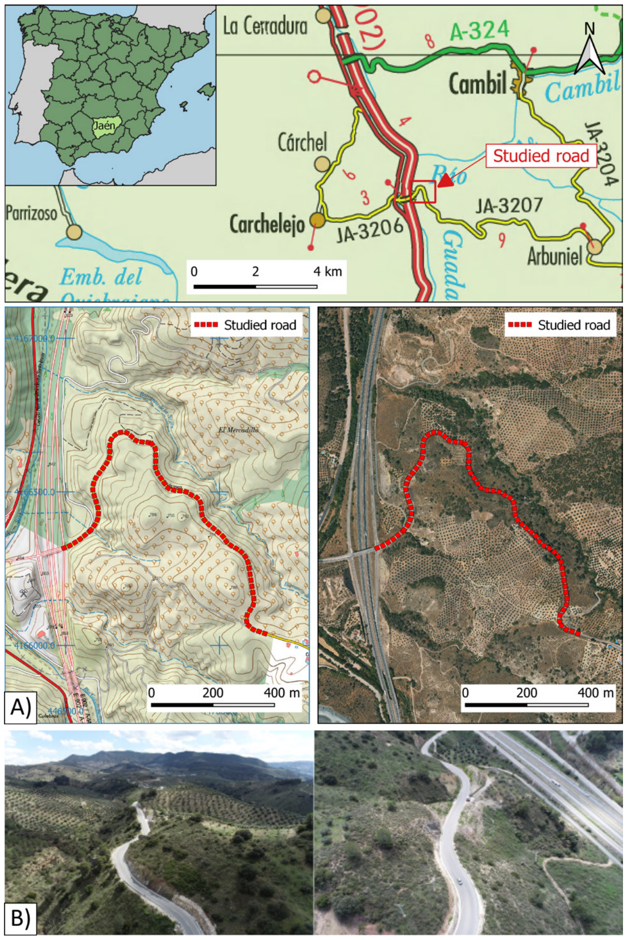

Figure 1. Area studied in this research: a) Maps displaying the studied road; b) aerial views of the road.

1.2 Objectives

This work presents a methodological study of data capture, processing, and fusion based on low-cost handheld MMS technology. The primary objective is to evaluate the efficiency and accuracy of these accessible systems and common processing applications for the monitoring of landslides and road slope stability. By analyzing the behavior of these sensors in complex environments, this study aims to provide a viable framework for rapid, cost-effective infrastructure risk management. Furthermore, the analysis aims to streamline the data acquisition process by proposing the use of these systems either as an alternative or integrated through data fusion with well-established techniques, such as TLS (Terrestrial Laser Scanning), or UAV-based LiDAR and photogrammetry. To optimize efficiency, systems originally designed for handheld operation or pole-mounting are deployed here in vehicle-mounted configurations. Additionally, this study explores a workflow that bypasses the need for external GNSS/RTK ground measurements—which are often cost-prohibitive in these projects—for both data processing and quality control. Instead, UAV-LiDAR data is utilized as the primary external reference for both control and validation purposes

2. Methodology

The methodology and analysis are based on the fundamental behaviour of errors inherent in this type of instrumentation (Keitaanniemi et al, 2023). These systems are originally optimized for handheld use at low speeds (<10 km/h) and minimal vibrations, which mitigates LiDAR distortion and sensor synchronization issues. Furthermore, their primary focus is on trajectory estimation derived from LiDAR or visual sensors, where loop closure plays a critical role in mitigating drift and object deformation. In scenarios where GNSS processing (RTK/PPK) is feasible, the trajectory calculation becomes more robust; it serves as a baseline to be integrated with IMU data and LiDAR/Visual-SLAM algorithms. This integration determines the trajectory positions at the high frequency required by the primary sensor (LiDAR) to generate the final point cloud. It is hypothesized that the primary errors in the point cloud will manifest in overlapping areas (regions captured at different times and perspectives) and as drifts that cause scale and shape deformations in the surveyed objects

The general workflow of the proposed methodology is illustrated in Figure 2. MMS data acquisition is performed using a vehicle-mounted instrument. Two cost-effective and accessible mounting configurations are proposed for analysis: a pole-mounted setup and a suction-cup-based configuration. Data acquisition follows a double-pass strategy (round trip) along the studied road section. Additionally, a GNSS base station is deployed to record RINEX data for post-processing.

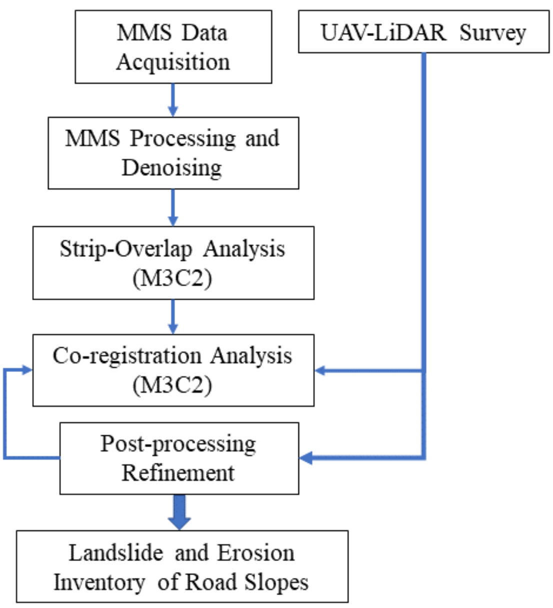

Figure 2. Proposed methodological workflow for the capturing processing and analysis of the MMS data for road slope stability monitoring.

Post-acquisition, data processing is conducted using the instrument's proprietary software. Two processing workflows are compared: one utilizing both GNSS base station and MMS data for PPK trajectory estimation and subsequent point cloud generation, and another bypassing GNSS information to simulate scenarios with degraded signals or the absence of a base station. The resulting data undergoes denoising to remove outliers such as hight vegetation, vehicles, or other artifacts. This is achieved through distance, intensity and segmentation filters to enhance subsequent comparative analyses. The methodology integrates external data from well-established massive capture techniques, specifically UAV-LiDAR, which serves both as a reference for analysis and for the registration and refinement process.

Following the initial phases, two distinct analysis workflows are implemented to evaluate the resulting point clouds. Both processes rely on point-to-point comparative analysis using the M3C2 algorithm (Lague et al., 2013), assessing the statistical distribution of distances between clouds and performing visual inspections via distance-based color-coded scalar fields. The first analysis focuses on strip-to-strip alignment; to achieve this, the point cloud is partitioned into the two separate strips performed during acquisition. This stage is critical for detecting misalignments and identifying double-points clouds artifacts.

Subsequently, the MMS point clouds are compared against the UAV-LiDAR reference data. In cases where GNSS-PPK processing was not utilized, a cloud-to-cloud registration is executed using the UAV-LiDAR dataset as the target. This comparative approach enables the identification of issues related to sensor drift and geometric deformations that compromise the georeferencing accuracy and structural fidelity of the data. Once the statistical and visual assessments are complete, the primary errors are characterized. If these discrepancies are deemed significant for multi-temporal change detection, a refinement process is then initiated.

This refinement aims to correct errors in overlapping areas (loop closures) and deformations caused by sensor drift. The procedure involves segmenting the point cloud into fixed-size sections, assuming uniform error distribution within each segment. These segments are then registered to the target cloud (UAV-LiDAR or corrected MMS) using Iterative Closest Point (ICP) algorithms (Besl and McKay, 1992). This iterative adjustment continues until the results meet the accuracy requirements for multi-temporal analysis. Finally, the methodology concludes with the detection and inventory of landslides and erosion on the road slopes.

3. Application and Results

3.1 UAV-LiDAR Survey

Reference data for point cloud analysis and refinement were acquired using a UAV-LiDAR system, specifically the Zenmuse L1 sensor mounted on a DJI Matrice 300 RTK platform. The survey was conducted in March 2025 at an altitude of 70 m above ground level (AGL), yielding an initial point cloud with an average point spacing of 5 cm (Figure 3a). Initial processing and automated classification of ground and non-ground points (Figure 3b) were performed using DJI Terra v4.2.5. To enhance strip alignment and reduce noise, StripAlign v2.7 was utilized. Further refinement of the data classification was carried out using Maptek I-Site PointStudio v2025.1. The final outputs consist of a reference point cloud with a decimated mean spacing of 10 cm and 3D ground model (Figure 3c).

3.2 MMS Survey

The MMS employed in this research is the CHCNAV RS10 (CHC Navigation) (Figure 4). Two distinct data acquisition campaigns were conducted using different mounting configurations. The first campaign, carried out in November 2024, utilized a 2-meter survey pole installation (Figure 5a). The average transit speed was 10 km/h, with a total acquisition time of approximately 15 minutes for the 1.3 km round trip. While this setup ensures high clamping security, the instrument is susceptible to significant operational vibrations.

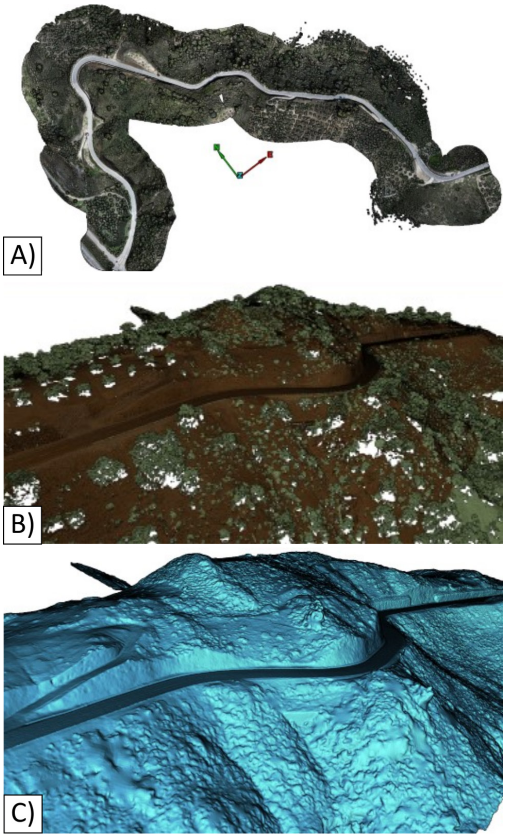

Figure 3. UAV-LiDAR survey results; a) point cloud: b) ground, non-ground classification; c) 3D Model.

Figure 4. Different views of the MMS CHCNAV RS10.

The second campaign was conducted in March 2026, using a suction-cup mounting system (Figure 5b). In this stage, two separate strips were performed at different speeds: 10 km/h and 20 km/h, with acquisition durations of 15 and 8 minutes, respectively. This configuration provides greater system stability; however, it requires careful verification of the suction cups' load-bearing capacity relative to the system's weight and the planned vehicle speed.

Table 1 provides a summary of the acquired data and the datasets employed to implement the proposed methodology. The primary objective is to evaluate which mounting configuration yields superior results, comparing the 2-meter survey pole (November 2024) (D24RTK) against the vehicle-integrated suction-cup system (March 2026). Furthermore, the impact of acquisition speed is assessed by comparing datasets captured at 10 km/h and 20 km/h (D26RTK10 and D26RTK20). Additionally, the study simulates a scenario where GNSS-based processing is unavailable or obstructed. For this GNSS-denied simulation, the dataset acquired at 10 km/h in March 2026 (D26SLAM10) was selected as the baseline to test the robustness of the SLAM-based trajectory and subsequent point cloud accuracy.

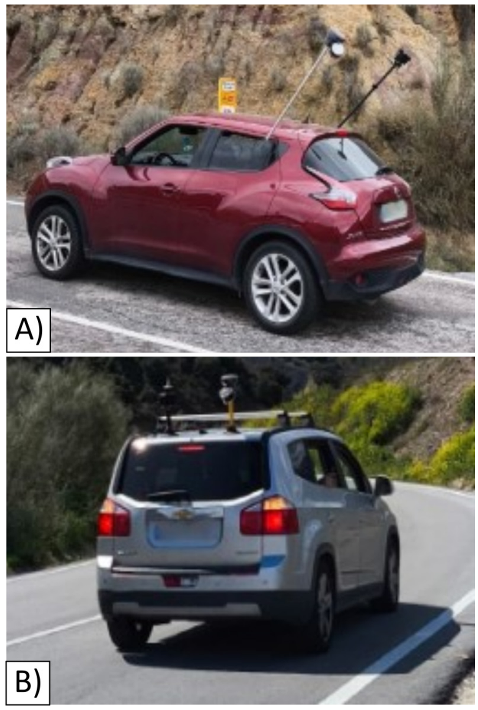

Figure 5. MMS mounting configurations: a) 2-meter pole mount; b) suction-cup mount.

Dataset	Pt Spacing [m]	Duration [min]
D24RTK	0.03	15
D26RTK10	0.02	15
D26RTK20	0.03	8
D26SLAM10	0.02	15

Table 1: summary of the datasets.

3.3 Strip Overlap Analysis

Following data acquisition, processing is conducted using the CHCNAV CoPre2 v2.10 software (Figure 6a). This platform supports three processing modes: RTK, PPK, and SLAM. While the PPK mode—which requires GNSS base station observation data—is the recommended workflow, our analysis evaluates both the PPK and SLAM-only modes. The software also provides advanced point cloud filtering based on range and intensity, alongside a noise reduction module. For all experimental campaigns, a maximum range filter of 60 m was applied in conjunction with the noise reduction algorithm. Post-processing quality control and further denoising were performed using CloudCompare v2.13, specifically utilizing the 'Label Connected Components' segmentation tool to remove outliers. The resulting outputs consist of a filtered point cloud and its corresponding trajectory file for each defined dataset. To conclude the processing stage, each cloud is partitioned into separate outbound and inbound strips to facilitate the subsequent strip-to-strip alignment analysis (Figure 6b).
The strip-to-strip analysis was conducted using the M3C2 plugin within CloudCompare v2.13. A distance range of ±20 cm was established as the maximum allowable threshold for inter-

strip discrepancies. Distances exceeding this range are categorized as erroneous data or points captured in only one of the two strips. Figure 7 illustrates the point clouds colored by their relative distance (scalar fields), while Table 2 summarizes the corresponding statistical indicators for each dataset.

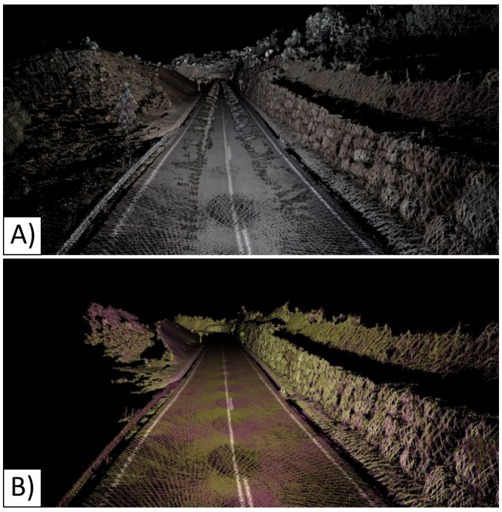

Figure 6. Point cloud processing workflow: a) raw point cloud generated via CoPre processing; b) results of the denoising stage, distinct colors represent the individual strips.

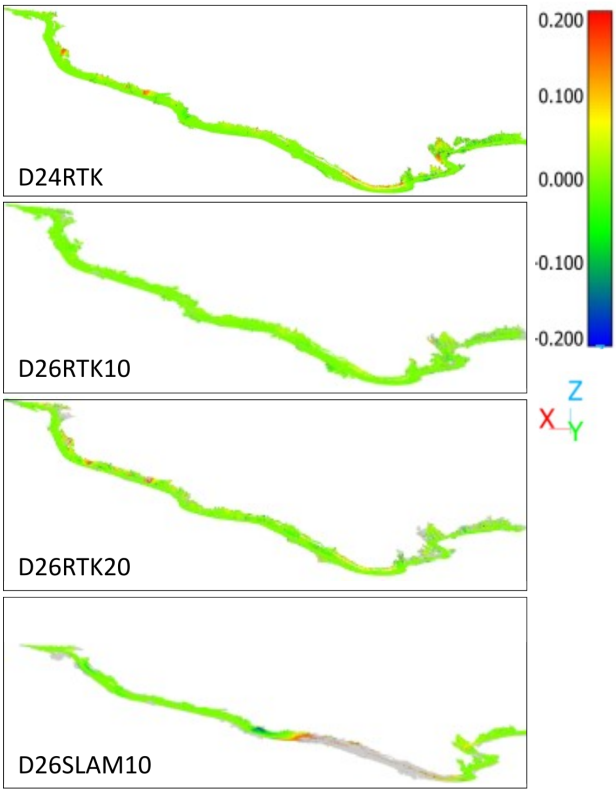

Figure 7. Point clouds coloured by M3C2 distances.

Visual inspection of the distance-colored point clouds reveals specific areas of deviation in the D24RTK and the D26RTK20 datasets, primarily corresponding to the regions highlighted in red. In the D26SLAM10 dataset, the gray-coded areas exhibit gross errors on the order of one meter between strips, indicating significant systematic drift in those sectors. In contrast, the D26RTK10 dataset shows no evidence of gross errors throughout the entire road section.

Statistically, with the exception of the SLAM-only dataset, over 90% of the points fall within the established ±20 cm threshold. For the D26SLAM10 case, approximately 30% of the data points lie outside this range. Consequently, the associated statistical indicators (mean and standard deviation) do not account for this significant percentage of outliers, rendering them unrepresentative and misleadingly suggesting a better result than actually achieved. For the remaining datasets, the mean distance values are near zero, indicating an absence of systematic bias between clouds, while the standard deviation remains consistent with the sensor resolution, confirming low noise levels in the final point clouds.

Dataset	%Pts in Range	Mean [m]	Stdev [m]
D24RTK	98.7%	0.000	0.026
D26RTK10	99.3%	0.001	0.018
D26RTK20	94.0%	0.003	0.032
D26SLAM10	73.4%	0.009	0.039

Table 2. M3C2 Strip-overlaps statistics: range ±20cm.

3.4 Co-registration and Multitemporal Analysis

Similar to the previous stage, a spatial filtering process is first applied to homogenize the point cloud densities. Specifically, a spatial decimation was performed to achieve a mean point spacing of 5 cm across all datasets. The comparative analysis is conducted using the UAV-LiDAR data as the reference (Ground Truth). For the D26SLAM10 dataset, the co-registration was executed using Maptek PointStudio v2025.1 to ensure geometric consistency with the reference frame. The analysis maintains the previously established ±20 cm threshold, under the assumption that significant topographic changes—such as landslides and erosion processes—will manifest as displacements exceeding this value. The comparative results, including the spatial distribution of discrepancies and statistical summaries, are presented in Table 3 and Figure 8.

Dataset	%Pts in Range	Mean [m]	Stdev [m]
D24RTK	90.1%	0.010	0.057
D26RTK10	86.8%	-0.004	0.059
D26RTK20	88.4%	0.010	0.058
D26SLAM10	25.5%	-0.010	0.100

Table 3. M3C2 Co-registration analysis: range ±20cm.

Post-analysis results for the D24RTK, D26RTK10, and D26RTK20 campaigns reveal specific areas with significant deviations for multitemporal calculations, particularly in the latter dataset. As indicated by the red rectangles in Figure 8, these discrepancies are concentrated at the beginning and end of the strips, coinciding with where the vehicle performs U-turns or changes direction. Furthermore, areas previously identified with double-surface artifacts also exhibit substantial deviations. Regarding the D26SLAM10 dataset, in addition to inter-strip misalignments, a pronounced systematic drift causes considerable geometric deformations throughout the point cloud. In this case, the statistical indicators align with the visual evidence, showing a standard deviation (σ) slightly higher than the average point spacing. These findings lead to several conclusions: first, the optimal configuration is the suction-cup mount at 10 km/h. Second, while other setups (excluding SLAM-only) may be suitable for the study, they are limited by localized significant errors. Consequently, to ensure a robust multitemporal analysis and accurate feature inventory, a point cloud refinement process is implemented. This additional stage

https://doi.org/10.5194/isprs-archives-XLIX-B2-2026-405-2026 | © Author(s) 2026. CC BY 4.0 License.

will also determine whether SLAM-processed data can be rendered viable for high-precision monitoring.

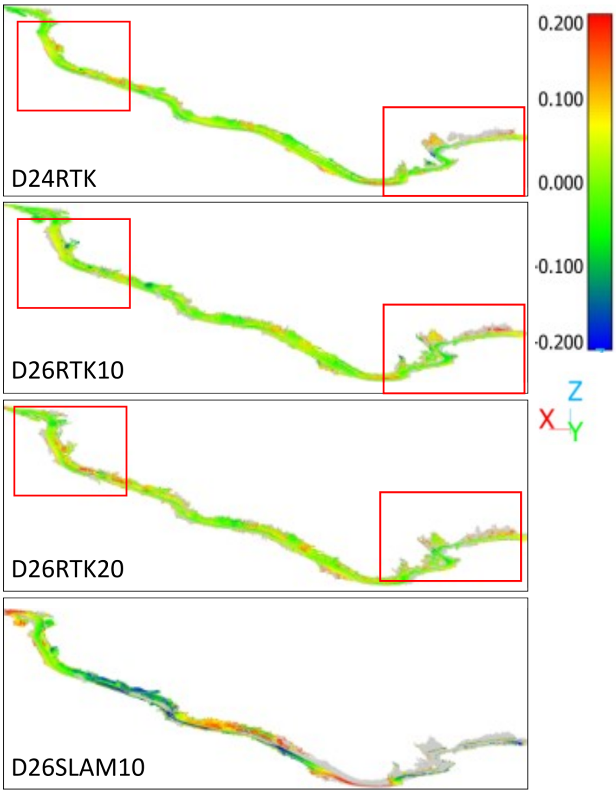

Figure 8. Point clouds coloured by M3C2 distances.

3.5 Refinement Processing

The refinement strategy is tailored based on the specific errors identified in the previous analysis. For the D24RTK, D26RTK20, and D26SLAM10 datasets, the refinement aims to correct both inter-strip misalignments and co-registration deviations. A segmentation length of 50 m was established for the first two cases, while the D26SLAM10 dataset underwent a comparative sensitivity analysis using segment lengths of 100 m, 50 m, and 20 m (D26SLAM10-100m, D26SLAM10-50m and D26SLAM10-20m). In contrast, for the D26RTK10 dataset, refinement focused on optimizing the co-registration with a coarser segmentation of 100 m. For datasets requiring both strip and co-registration refinement, the workflow begins by segmenting one of the strips (either outbound or inbound) and registering each segment to the UAV-LiDAR reference. Once this primary pass is corrected, it serves as the reference for the second pass's refinement. For the D26RTK10 dataset, the correction involves segmenting both strips simultaneously and registering them directly against the UAV-LiDAR ground truth. This automated refinement process was implemented via a Python script utilizing the point-cloud-registration library (https://github.com/scomup/point-cloud-registration). The Voxelized Point-to-Plane ICP (Iterative Closest Point) algorithm (Li, J. et al, 2022) was selected for the registration, as it provides superior convergence and robustness in in this type of scenario. The results obtained after the inter-strip correction (strip-alignment) for the selected datasets are presented in Table 4.

The results presented in Table 4 demonstrate a significant improvement in data quality, most notably within the D26SLAM10 dataset. The analysis indicates that a segmentation length of 50 m (D26SLAM10-50m) is sufficient to effectively correct the identified geometric discrepancies.

Dataset	%Pts in Range	Mean [m]	Stdev [m]
D24RTK	99.1%	-0.001	0.018
D26RTK20	96.0%	-0.003	0.023
D26SLAM10-100m	96.5%	0.003	0.033
D26SLAM10-50m	96.7%	0.001	0.015
D26SLAM10-20m	96.6%	0.001	0.014

Table 4. M3C2 Strip overlaps statistics: range ±20cm.

Furthermore, the outcomes of the refinement process aimed at enhancing georeferencing accuracy are illustrated in Figure 9 and summarized in Table 5. Overall, these results show a marked reduction in standard deviation values, which are now on the order of the mean point spacing (5 cm) of the analysed point clouds. The most significant improvement is observed in the D26SLAM10; following the refinement, its status was upgraded from unsuitable to fully viable for landslide detection and monitoring applications.

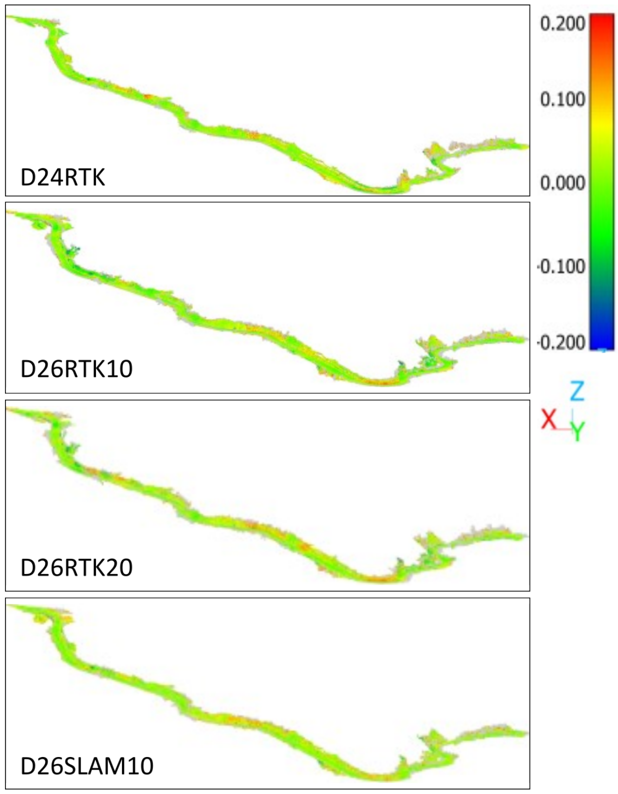

Figure 9. Point clouds coloured by M3C2 distances.

Dataset	%Pts in Range	Mean [m]	Stdev [m]
D24RTK	91.57%	0.000	0.043
D26RTK10	87.65%	-0.001	0.050
D26RTK20	89.51%	-0.002	0.049
D26SLAM10	90.16%	0.001	0.046

Table 5. M3C2 Co-registration analysis: range ±20cm.

3.6 Multitemporal analysis for landslide and erosion detection

The multitemporal analysis follows a workflow similar to the previous stages, utilizing the same software suite but adopting a cloud-to-model (C2M) comparison approach. In this phase, the D24RTK dataset serves as the baseline, as it represents the earliest acquisition campaign. This dataset underwent a ground/non-ground classification process to extract the bare-earth points, from which a 3D surface model (Mesh/TIN) was generated for the analysis.

Figure 10 illustrates the results of an embankment section exhibiting erosion defects. By utilizing the refined and corrected datasets, the multitemporal comparison demonstrates high consistency across all acquisition modes, yielding nearly identical results in terms of detected volumetric changes and spatial distribution of the erosion.

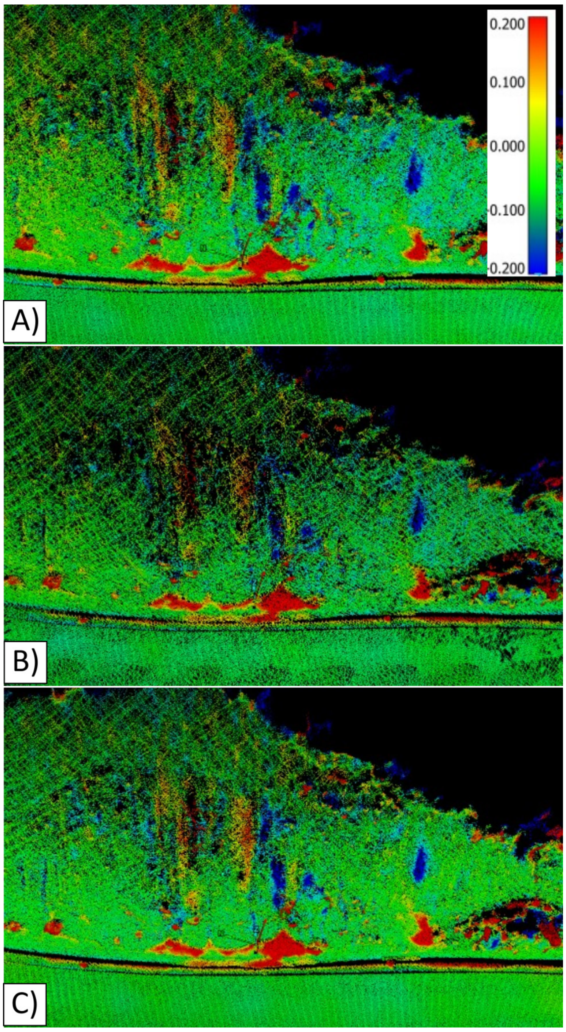

Figure 10. Point cloud coloured by M3C2 distances: a) D24RTK vs D26RTK10; b) D24RTK vs D26RTK20; c) D24RTK vs D26SLAM10.

Figure 11 illustrates several instability features and erosion patterns detected along the study section, which were triggered by the intense precipitation events recorded during early 2026. These changes, identified through the multitemporal comparison of the refined MMS datasets, demonstrate the system's capacity for high-resolution monitoring of road infrastructure after extreme weather events.

4. Conclusions

Recent algorithmic advancements have established handheld mobile mapping systems (HMMS) as a highly versatile tool for a wide range of geomatic projects. This study demonstrates that, in general terms, these vehicle-mounted sensors are fully capable of performing road slopes monitoring. Systems such as the CHCNAV RS10, which integrate GNSS, IMU, cameras, and LiDAR, provide robust results in scenarios with adequate satellite visibility, often meeting accuracy requirements without the need for additional post-processing refinement. To facilitate this, two vehicle-mounting configurations—survey poles and suction cups—are proposed. Due to their simplicity and universal design, these mounting solutions can be easily adapted to most similar HMMS platforms currently available on the market.

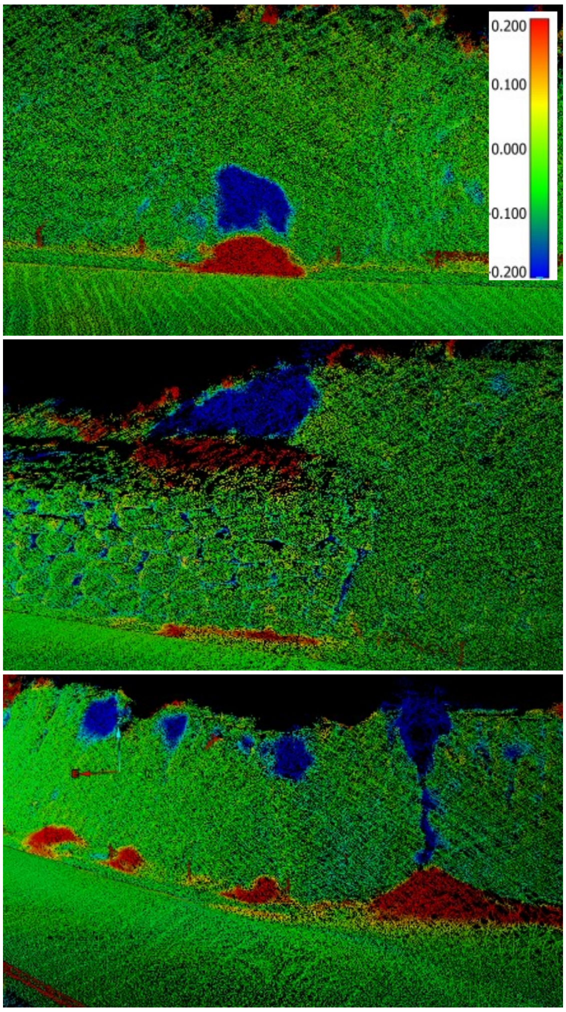

Figure 11. Examples of point cloud coloured by M3C2 distances in areas with erosion.

Experimental results confirm that the suction-cup mounting system provides superior stability compared to the traditional 2-meter survey pole, which is highly susceptible to operational vibrations. Regarding acquisition speed, while 10 km/h remains the benchmark for maximum precision, the 20 km/h configuration is viable for rapid inventory. However, these setups may still be affected by double-surface artifacts or trajectory drift in certain sections.

In GNSS-denied scenarios, where satellite data cannot be integrated into the SLAM process, the resulting systematic drift prevents reliable multitemporal analysis and continuous monitoring of road embankments. This is primarily due to the geometric deformation generated in the final data after the SLAM process; the resulting point cloud deviates considerably from reality. To address this, a refinement methodology is proposed to correct or significantly reduce these geometric

https://doi.org/10.5194/isprs-archives-XLIX-B2-2026-405-2026 | © Author(s) 2026. CC BY 4.0 License.

discrepancies, enabling the use of datasets that would otherwise be discarded. Following the point cloud refinement, the monitoring results from both campaigns demonstrate the system's capacity to accurately inventory landslides and erosion phenomena affecting the studied road slopes.

Future work will focus on scaling the proposed refinement methodology to extensive road networks. While this study validated the workflow on a 1-kilometer pilot section, increasing the analysis distance to tens of kilometers presents new challenges in terms of data management and computational efficiency. Furthermore, this expansion will be critical to assess the long-term performance of HMMS across diverse geographical terrains and varying GNSS conditions, ultimately providing a robust solution for regional infrastructure asset management.

Acknowledgements

The authors would like to acknowledge the support provided by the Instituto de Estudios Giennenses (IEG) and Diputación Provincial de Jaén throughout the research project MMS-ROAD and the support of Centro de Estudios Avanzados en Ciencias de la Tierra, Energía y Medio Ambiente (University of Jaén).

References

Al-Bayari, O., 2019. Mobile Mapping Systems in civil engineering projects (case studies). *Applied Geomatics*, 11, 1-13. doi.org/10.1007/s12518-018-0222-6

Besl, P.J. McKay, N.D., 1992. A Method for Registration of 3D Shapes. *IEEE Transactions on Pattern Analysis and Machine Intelligence*, 14(2), 239-256.

Clague, J.J., 2013: Landslide. In: P.T. Bobrowsky (Editor), *Encyclopedia of natural hazards* (Vol. 1135). Springer, Dordrecht, the Netherlands, pp. 594-602.

Debeunne, C., Vivet, D., 2020. A Review of Visual-LiDAR Fusion based Simultaneous Localization and Mapping. *Sensors*, 20, 2068. doi.org/10.3390/s20072068

Elhashash, M., Albanwan, H., Qin, R., 2022. A review of mobile mapping systems: From sensors to applications. *Sensors*, 22, 4262. doi.org/10.3390/s22114262

Fernández, T., Pérez, J.L., Gómez, J.M., Cardenal, J., Moya, F., Delgado, J., 2021. Multitemporal landslide inventory and activity analysis by means of aerial photogrammetry and LiDAR techniques in an area of Southern Spain. *Remote Sensing*, 13(11), 2110. doi.org/10.3390/rs13112110

Huang, L., 2021: Review on LiDAR-based SLAM techniques. *Proceedings of the 2021 International Conference on Signal Processing and Machine Learning (CONF-SPML)*, Stanford, USA, pp. 163-168.

Hussain, Y., Schlögel, R., Innocenti, A., Hamza, O., Iannucci, R., Martino, S., Havenith, H.-B., 2022. Review on the Geophysical and UAV-Based Methods Applied to Landslides. *Remote Sensing*, 14, 4564. doi.org/10.3390/rs14184564

Kalenjuk, S., Lienhart, W., 2022. A method for efficient quality control and enhancement of mobile laser scanning data. *Remote Sensing*, 14(4), 857. doi.org/10.3390/rs14040857

Kazerouni, I.A., Fitzgerald, L., Dooly, G., Toal, D., 2022. A survey of state-of-the-art on visual SLAM. *Expert Systems with Applications*, 205, 117734. doi.org/10.1016/j.eswa.2022.117734

Keitaanniemi, A., Rönnholm, P., Kukko, A., Vaaja, M.T., 2023. Drift analysis and sectional post-processing of indoor simultaneous localization and mapping (SLAM)-based laser scanning data. *Automation in construction*, 147, 104700. doi.org/10.1016/j.autcon.2022.104700

Kovanič, Ľ., Topitzer, B., Peťovský, P., Blišťan, P., Gergeľová, M. B., Blišťanová, M., 2023. Review of photogrammetric and lidar applications of UAV. *Applied Sciences*, 13(11), 6732. doi.org/10.3390/app13116732

Lague, D., Brodu, N., Leroux, J., 2013. Accurate 3D Comparison of Complex Topography with Terrestrial Laser Scanner: Application to the Rangitikei Canyon (N-Z). *ISPRS J. Photogramm. Remote Sens.*, 82, 10-26. doi.org/10.1016/j.isprsjprs.2013.04.009

Li, J., Zhan, J., Zhou, T., Bento, V.A., Wang, Q., 2022. Point cloud registration and localization based on voxel plane features. *ISPRS Journal of Photogrammetry and Remote Sensing*, 188, 363-379. doi.org/10.1016/j.isprsjprs.2022.04.017.

Mat Zam, P.M., Fuad, N.A., Yusoff, A.R., Majid, Z., 2018. Evaluating the performance of terrestrial laser scanning for landslide monitoring. *Int. Arch. Photogramm. Remote Sens. Spatial Inf. Sci.*, 42, 35-55. doi.org/10.5194/isprs-archives-XLII-4-W9-35-2018

Raper, J., 2009: GIS, Mobile and Locational Based Services. In: R. Kitchin, N. Thrift (Editors), *International Encyclopedia of Human Geography*. Elsevier, Oxford, United Kingdom, pp. 513-519.

Sun, J., Yuan, G., Song, L., Zhang, H., 2024. Unmanned Aerial Vehicles (UAVs) in Landslide Investigation and Monitoring: A Review. *Drones*, 8(1), 30. doi.org/10.3390/drones8010030

Szeliski, R., 2011. *Computer Vision: Algorithms and Applications*. Springer, London.

Türk, Y., Özçelik, V., Akduman, E., 2024. Capabilities of using UAVs and close range photogrammetry to determine short-term soil losses in forest road cut slopes in semi-arid mountainous areas. *Environmental Monitoring and Assessment*, 196(2), 149. doi.org/10.1007/s10661-024-12339-1

Westoby, M.J., Brasington, J., Glasser, N.F., Hambrey, M.J., Reynolds, J.M., 2012. 'Structure-From-Motion' photogrammetry: A low-cost, effective tool for geoscience applications. *Geomorphology*, 179, 300-314. doi.org/10.1016/j.geomorph.2012.08.021

Zhang, Z., Zhu, L., 2023. A review on unmanned aerial vehicle remote sensing: Platforms, sensors, data processing methods, and applications. *Drones*, 7(6), 398. doi.org/10.3390/drones7060398